Solar-Terrestrial Physics. 2025, vol. 11, iss. 4, pp. 3–13. DOI: 10.12737/stp-114202501. © 2025 L.L. Kitchatinov. Published by INFRA-M Academic Publishing House

DOI: 10.12737/stp-114202501

Received 29.05.2025
Accepted 15.07.2025

LARGE-SCALE FLOW MODEL FOR SOLAR AND STELLAR CONVECTION ZONES

L.L. Kitchatinov
Institute of Solar-Terrestrial Physics SB RAS,
Irkutsk, Russia, kit@iszf.irk.ru

Abstract. The paper presents a mean-field model for large-scale flows in convection zones of the Sun and solar-type stars. The model extends former differential rotation models by allowance for variations of the flow with time and its deviation from axial symmetry. The model is realized as a numerical code, which combines the spectral method of decomposition in spherical functions with second-order accurate finite-difference method for time and radius. First computations show close agreement of the axially symmetric part of the computed flow with helioseismological detections of differential rotation and meridional circulation. Patterns of the time-decaying non-axisymmetric flow computed with the model qualitatively agree with the Rossby waves observed on the Sun. The paper also formulates a problem for further development of the large-scale flow theory.

Keywords: Sun, stars, rotation, convection, turbulence, numerical methods.

INTRODUCTION

The Sun and solar-type stars host large-scale flows, inhomogeneous (differential) rotation and meridional circulation being the most known examples. The rotation rate increases from poles to the equator by about 30% on the Sun, and the surface meridional flow from the equator to the poles has an amplitude ~10 m/s. The large-scale flows are important for the solar and stellar dynamos [Charbonneau, 2020; Karak, 2023; Charbonneau, Sokoloff, 2023].

The large-scale flows are, by all probabilities, driven by turbulent convection. This is clearly indicated by spatial coincidence of the regions occupied by the differential rotation [Thompson et al., 1996; Schou et al., 1998] and meridional flow [Rajaguru, Antia, 2015; Gizon et al., 2020] with the convection zone as revealed by helioseismology.

The large-scale flow theory is dominated by two complementary approaches. A majority of studies apply the so-called direct numerical simulations. In this approach, three-dimensional time-dependent flows comprising both convection and large-scale parts are computed from the equations of hydrodynamics. The large-scale flow can be extracted by time averaging. A reproduction of observations with such an approach would confirm the fact that the Sun obeys fundamental equations. In spite of impressive progress in this direction, a correspondence to observations is still not achieved (see, e.g., reviews by Hotta et al. [2023] and Käpylä et al. [2023]).

Another approach, named “mean-field theory”, differs by sequence of averaging and equation solving (see, e.g., Rüdiger [1989], Brandenburg et al. [2023]). Averaging of fundamental equations is done first. This gives equations for large-scale fields. The equations include contributions of turbulence, which should be expressed in terms of sufficiently simple turbulence parameters and the averaged large-scale fields. Approximate methods of turbulence theory and not well justified assumptions are unavoidable in this approach, but the mean-field theory clarifies the physics of large-scale flows.

The numerical models based on the mean-field theory [Kitchatinov, Olemskoy, 2011, 2012] reproduce the differential rotation and meridional flow detected by helioseismology and do not contradict the observed [Barnes, 2005; Balona, Abedigamba, 2016] dependences of the differential rotation on rotation rate and temperature of solar-type stars. The models compute the large-scale flows in stellar convective envelopes assuming their axial symmetry and independence of time. There are, however, dynamical models of torsional oscillations [Pipin, Kosovichev, 2019, 2020].

This paper extends the mean-field models with allowance for the large-scale flow dependence on time and longitude. Observations of large-scale vortical flows on the Sun [Löptien et al., 2018] justify the expediency of such an extension. A planned unification of differential rotation and stellar dynamo models also demands allowance for the variability with time. Stellar torsional oscillations can be strong [Collier Cameron, Donati, 2002] and large deviations from axial symmetry can be expected [Kitchatinov, 2022].

The model design is described in Section 1. Section 2 explains the numerical method used in the model. Results of the first applications to the Sun are given in Section 3. Main results and a problem for future are summarized in Conclusions.

1. MODEL

1.1. Basic equations and approximations

The model confines to the case of slow rotation, where the centrifugal acceleration $R_*\Omega^2$ is small compared to the gravity g and deviation from spherical symmetry in distributions of density ρ, temperature T,

and pressure $P=\left(c_{\rm p}-c_{\rm v}\right)\rho T$ can be neglected (Ω is the angular velocity, R_* is the stellar radius, $c_{\rm p}$ and $c_{\rm v}$ are the specific heat capacity at constant pressure and volume; perfect gas equation of state is assumed). The spherical symmetry assumption does not, however, refer to the specific entropy $S=c_{\rm v}\ln P-c_{\rm p}\ln\rho$, whose small spatial inhomogeneity is responsible for thermal convection. The temperature gradient in stellar convection zones is superadiabatic, but the relative value of superadibaticity,

$$\in=\frac{r}{c_{\rm p}}\left|\nabla S\right|=\frac{r}{T}\left|\nabla T-\left(\nabla T\right)_{\rm ad}\right|\ll 1. \qquad (1)$$

is small. In this equation, r is the distance to the star's center, $\left(\nabla T\right)_{\rm ad}=\mathbf{g}/c_{\rm p}$ is the adiabatic gradient, the equation of state and the hydrostatic equilibrium condition, $\nabla P=\rho\mathbf{g}$ were used. An estimation of $\in$ (1) confirming its small value will be given below.

At small superadiabaticity, the velocity $\mathbf{u}$ of turbulent convection and the mean large-scale flow velocity $\mathbf{v}$ are both small compared to the sound velocity. The large radial inhomogeneity of the fluid does not, however, permit the incompressibility approximation. It is replaced by the anelastic approximation, which in particular means the divergence-free of the momentum density, $\mathrm{div}\left(\rho\mathbf{v}\right)=0$. The physics of anelastic approximation and its justification are clearly explained by Lantz and Fan [1999]. The large-scale flow equation in this approximation can be written as follows

$$\frac{\partial\mathbf{v}}{\partial t}=-\left(\mathbf{v}\cdot\nabla\right)\mathbf{v}+\frac{1}{\rho}\nabla\cdot\mathbf{R}+ \\ +2\mathbf{v}\times\mathbf{\Omega}-\nabla\left(\frac{P'}{\rho}\right)-\frac{S}{c_{\rm p}}\mathbf{g}. \qquad (2)$$

In this equation, $\mathbf{R}$ is the Reynolds stress tensor, $R_{ij}=-\rho<u_iu_j>$, where the angular brackets mean averaging, and $\nabla\cdot\mathbf{R}$ is a vector with components ∇_jR_{ij}, where the repetition of subscripts from here on signifies summation. Equation (2) refers to the reference frame co-rotating with a star with angular velocity $\mathbf{\Omega}$.

In the anelastic approximation, all thermodynamic parameters except entropy are considered to be steady functions of coordinates [Lantz, Fan, 1999]. Distribution of these parameters within the convection zone is taken from the model MESA [Paxton et al., 2011] of stellar structure and evolution as it is explained in Section 2 below. Entropy is a dependent variable in our model. It obeys the heat transport equation

$$\frac{\partial S}{\partial t}=-\left(\mathbf{v}\cdot\nabla\right)S+\frac{1}{\rho T}\nabla_i\rho T\chi_{ij}\nabla_jS- \\ -\frac{1}{\rho T}\nabla\cdot\mathbf{F}^{\rm rad}+\frac{q}{\rho T}, \qquad (3)$$

where $\mathbf{\chi}$ is the thermal diffusivity tensor, q stands for the sources/sinks of heat (due to nuclear reactions within the convection zone, gravitational energy release by stellar compression and others), and $\mathbf{F}^{\rm rad}$ is the radiative heat flux. With the accepted approximations, it reads

$$\mathbf{F}^{\rm rad}=-\mathbf{g}\frac{16\sigma T^3}{3\rho c_{\rm p}\kappa}, \qquad (4)$$

where σ is the Stefan — Boltzmann constant and κ is the opacity.

The Reynolds stress and thermal diffusivity in Equations (2) and (3) should be expressed in terms of the fluid parameters and large-scale fields.

1.2. Turbulent transport coefficients in rotating convection zone

The key parameter for the rotational influence on convective turbulence is the Coriolis number,

$$\Omega^*=2\tau\Omega, \qquad (5)$$

where $\tau=\ell/u$ is the characteristic time of turbulent mixing and u is the root-mean-square velocity. Let us estimate τ for non-rotating convection. This can be done with the mixing-length theory (see, e.g., the recent review by Joyce and Tayar [2023]), on which the computations of convection zone structure in stellar evolution models and the anelastic approximation [Lantz, Fan, 1999] are based. The mixing-length estimation for the RMS velocity reads

$$u^2=-\frac{\ell^2g}{4c_{\rm p}}\frac{\partial S}{\partial r}, \qquad (6)$$

where $\ell=\alpha_{\rm MLT}H_{\rm p}$ is the mixing-length proportional to the pressure scale height $H_{\rm p}=P/\left(\rho g\right)$. The turbulent convection transports the heat flux $\delta F=L_*/\left(4\pi r^2\right)-F^{\rm rad}$:

$$-\rho T\chi_{\rm T}\frac{\partial S}{\partial r}=\delta F, \qquad (7)$$

where L_* is the total flux through the sphere of radius r. With allowance for Equation (6), the thermal diffusivity $\chi_{\rm T}=\ell u/3$ can be written as

$$\chi_{\rm T}=\frac{\ell^2}{6}\sqrt{-\frac{g}{c_{\rm p}}\frac{\partial S}{\partial r}}. \qquad (8)$$

On using Equation (7), this leads to the entropy gradient

$$-\frac{\partial S_0}{\partial r}=\left(\frac{c_{\rm p}}{g}\right)^{1/3}\left(\frac{6\delta F}{\rho T\,\ell^2}\right)^{2/3}, \qquad (9)$$

where the subscript in S_0 reminds that the equation does not account for rotation. Substitution of entropy gradient (9) into Equation (6) leads to an estimation of the convective turnover time:

$$\tau=\left(\frac{4c_{\rm p}\rho\ell^2T}{3g\delta F}\right)^{1/3}. \qquad (10)$$

This estimation is used to define Coriolis number (5). All the parameters in the right-hand side of (10) are taken from a stellar structure model (MESA in this paper). The convective time τ depends on the radius r and

increases with depth in the convection zone. Therefore, the Coriolis number also does so.

The quasilinear theory of turbulent transport gives for the thermal diffusivity tensor of Equation (3) the following expression

$$\begin{aligned}\chi_{ij} &= \chi\delta_{ij} + \chi_{\parallel}\widehat{\Omega}_i\widehat{\Omega}_j,\\ \chi &= \chi_{\mathrm{T}}\phi\left(\Omega^*\right),\\ \chi_{\parallel} &= \chi_{\mathrm{T}}C_{\chi}\phi_{\parallel}\left(\Omega^*\right),\end{aligned} \tag{11}$$

where C_χ is the model parameter ($C_\chi = 2$ in this paper) and $\widehat{\mathbf{\Omega}} = \mathbf{\Omega}/\Omega$ is the unit vector along the rotation axis. The functions $\phi\left(\Omega^*\right)$ and $\phi_{\parallel}\left(\Omega^*\right)$ are shown in Figure 1. Analytical expressions for these functions are given in Kitchatinov et al. [1994]. Equation (11) accounts for the rotationally induced anisotropy of turbulent heat transport. χ is the isotropic part of the thermal diffusion and $\chi_{\parallel}$ is the extra diffusivity along the rotation axis. Anisotropy of thermal diffusion is essential for differential rotation physics. Reproducing the results of helioseismology with theoretical models is only possible with allowance for this anisotropy [Rüdiger et al., 2005]. It can be seen in Figure 1 that the anisotropy vanishes in the slow rotation limit, $\Omega^* \to 0$, as should be the case.

Figure 1 also shows that rotation suppresses thermal diffusion. This rotational effect is partly compensated by an increase in the entropy gradient which leads to an increase in χ_{T} (8). In the steady model by Kitchatinov and Olemskoy [2011], S in Equation (8) was treated as a dependent variable, i.e. the nonlinear diffusion model was applied. In the present dynamical 3D model, nonlinear diffusion would require inversion of large matrixes that reduces considerably the computation rate. We therefore apply linear diffusion and treat χ_{T} of (8) as a given function of radius r, but the effect of the increase in entropy gradient in rotating fluid is nevertheless included by replacing $\partial S/\partial r$ in (8) with its corrected value,

$$\frac{\partial S}{\partial r} = \frac{\partial S_0/\partial r}{\sqrt{\phi\left(\Omega^*\right) + 0.2\phi_{\parallel}\left(\Omega^*\right)}}, \tag{12}$$

where $\partial S_0/\partial r$ is the gradient (9) for not rotating fluid.

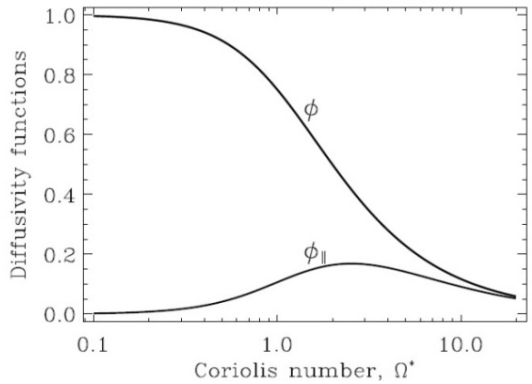

Figure 1. The functions $\phi\left(\Omega^*\right)$ and $\phi_{\parallel}\left(\Omega^*\right)$ of the dependence of thermal diffusivity (11) on rotation rate

Apart from thermal eddy diffusion, modelling large-scale flows demands a definition of the Reynolds stress tensor R_{ij} in Equation (2). Lebedinsky [1941] was probably the first to find that in addition to the well-known contribution by the eddy viscosity R_{ij}^{v} rotating anisotropic turbulence produces a non-dissipative stress R_{ij}^{Λ}:

$$R_{ij} = R_{ij}^{\mathrm{v}} + R_{ij}^{\Lambda}, \tag{13}$$

which can cause the Sun to rotate differentially. The Lebedinsky effect, later named the Λ-effect, has been thoroughly studied and confirmed by computations within the mean-field theory [Rüdiger, 1989]. Pictorial explanation of this effect can be found in Kitchatinov [2005]. The Lebedinsky [1941] theory is linear in the Coriolis number. This number is indeed small near the solar surface but increases with depth to be large near the base of the convection zone. The Λ-эффект of the turbulence anisotropy was found to be small ($\propto 1/\Omega^{*2}$) in the deep convection zone [Kichatinov, 1986]. The anisotropy can, however, be replaced by inhomogeneity of the fluid density. The density inhomogeneity does also produce the Λ-effect, which is not small for large Coriolis number [Kichatinov, 1987]. The anisotropy is nevertheless important. Only with allowance for anisotropy, the seismologically detected near-surface shear layer of solar rotation can be explained [Kitiashvili et al., 2023; Kitchatinov, 2023]. Therefore, the Λ-effect of the proposed model

$$\begin{aligned}R_{ij}^{\Lambda} = -\rho\Omega\Big\{&\Lambda_0\left[\hat{r}_i\left(\widehat{\mathbf{\Omega}}\times\hat{\mathbf{r}}\right)_j + \hat{r}_j\left(\widehat{\mathbf{\Omega}}\times\hat{\mathbf{r}}\right)_i\right] -\\ &-\Lambda_1\left(\hat{\mathbf{r}}\cdot\widehat{\Omega}\right)\left[\widehat{\Omega}_i\left(\widehat{\mathbf{\Omega}}\times\hat{\mathbf{r}}\right)_j + \widehat{\Omega}_j\left(\widehat{\mathbf{\Omega}}\times\hat{\mathbf{r}}\right)_i\right]\Big\}\end{aligned} \tag{14}$$

includes both the anisotropy and inhomogeneity. In this equation,

$$\begin{aligned}\Lambda_0 &= v_{\mathrm{T}}\left(\frac{\alpha_{\mathrm{MLT}}}{\gamma}\right)^2\lambda_0\left(\Omega^*\right),\\ \Lambda_1 &= v_{\mathrm{T}}\left(\frac{\alpha_{\mathrm{MLT}}}{\gamma}\right)^2\lambda_1\left(\Omega^*\right)\end{aligned} \tag{15}$$

are functions of radius r, $\gamma = c_{\mathrm{p}}/c_{\mathrm{v}}$ is the adiabaticity index, $\hat{\mathbf{r}} = \mathbf{r}/r$ is the radial unit vector, $v_{\mathrm{T}} = 0.8\chi_{\mathrm{T}}$ (quasilinear theory of turbulent transport gives the value of 0.8 for the Prandtl number), and

$$\begin{aligned}\lambda_0\left(\Omega^*\right) &= J_0\left(\Omega^*\right) + 2I_0\left(\Omega^*\right),\\ \lambda_1\left(\Omega^*\right) &= J_1\left(\Omega^*\right) + 2I_1\left(\Omega^*\right).\end{aligned} \tag{16}$$

The functions J_0 and J_1 account for the contribution of the density inhomogeneity. I_0 and I_1 stand for the contribution of turbulence anisotropy. The functions of Equation (16) are shown in Figure 2. Analytical expressions for the functions are given in [Kitchatinov, Rüdiger, 2005]. The contribution of λ_0 in (14) is responsible for the angular momentum transport in radius. Its negative value means the transport toward the star's center. The contribution of λ_1 gives the angular momentum transport along the rotation axis. Its positive value

means the transport from poles to the equator. The contribution of λ_0 dominates at small Ω^*, i.e. near the stellar surface. This is a possible reason for the increase in the rotation rate with depth beneath the surface of the Sun [Schou et al., 1998].

Figure 2 also shows the functions f_ν and f_μ for the dependence of turbulent viscosities on Ω^*. Similar to thermal diffusion, the eddy viscosity in a rotating fluid is anisotropic. The anisotropy of viscosity is less consequential for the large-scale flows compared to the anisotropy of thermal diffusion, but it causes many difficulties for numerical computations. The anisotropic viscosity can transform a toroidal non-axisymmetric flow into a poloidal one and the other way round. This effect of anisotropy links the equations for poloidal and toroidal flows, thus increasing the size of the matrixes for inversion and reducing the computation rate. The proposed model employs the dissipative Reynolds stress in (13) with isotropic viscosity

$$R_{ij}^{\nu} = \rho\nu\left(\nabla_i v_j + \nabla_j v_i\right) + \rho\mu\delta_{ij}\mathrm{div}\mathbf{v}, \qquad \nu = \nu_{\mathrm{T}} f_\nu\left(\Omega^*\right),\ \mu = \nu_{\mathrm{T}} f_\mu\left(\Omega^*\right). \tag{17}$$

The functions f_ν and f_μ are also shown in Figure 2. In a rotating fluid, the eddy viscosity coefficients differ between the directions along and across the rotation axis. The viscosity ν in (17) is a half-sum of the viscosities for these two directions. The eddy viscosity tensor for a rotating fluid was derived in [Kitchatinov et al., 1994] where analytical expressions for the functions $\phi_1\left(\Omega^*\right), \phi_2\left(\Omega^*\right)$, and $\phi_3\left(\Omega^*\right)$, from which the functions $f_\nu = \phi_1 + 0.5\phi_2$ and $f_\mu = \phi_3$ are constructed, are given.

1.3. Flow potentials and boundary conditions

The anelasticity condition, $\mathrm{div}\left(\rho\mathbf{v}\right) = 0$, imposes a restriction on the velocity field, which allows the velocity to be expressed in terms of two scalar potentials [Chandrasekhar, 1961],

$$\mathbf{v} = \frac{\hat{\boldsymbol{r}}}{\rho r^2}\left(\hat{L}V\right) - \frac{\hat{\boldsymbol{\vartheta}}}{r}\left(\frac{1}{\rho}\frac{\partial^2 V}{\partial r\partial\vartheta} + \frac{1}{\sin\vartheta}\frac{\partial W}{\partial\varphi}\right) - \frac{\hat{\boldsymbol{\varphi}}}{r}\left(\frac{1}{\rho\sin\vartheta}\frac{\partial^2 V}{\partial r\partial\varphi} - \frac{\partial W}{\partial\vartheta}\right). \tag{18}$$

In this equation, the usual spherical coordinates are used; $\hat{\boldsymbol{\vartheta}}$ and $\hat{\boldsymbol{\varphi}}$ are unit vectors in meridional and azimuthal directions, $V\left(r,\vartheta,\varphi\right)$ and $W\left(r,\vartheta,\varphi\right)$ are the poloidal and toroidal flow potentials respectively, and

$$\hat{L} = \frac{1}{\sin\vartheta}\frac{\partial}{\partial\vartheta}\sin\vartheta\frac{\partial}{\partial\vartheta} + \frac{1}{\sin^2\vartheta}\frac{\partial^2}{\partial\varphi^2} \tag{19}$$

is the angular part of the Laplacian.

Toroidal flow lines lie on spherical surfaces of constant radius r. The poloidal flow has a toroidal vector potential. In the proposed model, motion equation (2) is transformed into the equations for the flow potentials.

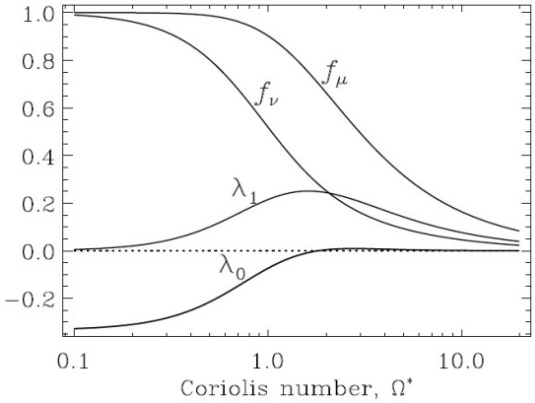

Figure 2. The functions from Equations (15)–(17), which control dependence of the Λ-effect and eddy viscosities on the rotation rate of a star

The radial component of curled Equation (2) gives the equation for the toroidal potential W. The radial component of Equation (2) curled twice gives the equation for the poloidal flow. This procedure for deriving the large-scale flow equations differs from that used in the dynamo theory, where the equation for poloidal magnetic field can be obtained as the radial component of the induction equation without double curling [Krause, Rädler, 1980]. The difference is due to the fact that divergence-free of the magnetic field is a fundamental law, but divergence-free of the momentum density is a consequence of the anelastic approximation. Curling the motion equation filters out the potential forces. The equations for the large-scale flow in terms of the scalar flow potentials are rather bulky. They are given in the Appendix.

A unique solution of the model equations demands the boundary conditions. Natural conditions for the large-scale flow are zero cross-components of the stress tensor, $R_{r\varphi} = R_{r\vartheta} = 0$ at the low (r_1) and upper (r_2) boundaries of the simulation region. The low boundary is placed at the base of the convection zone; and the upper one, at a small depth below the photosphere ($r_2 = 0.97R_*$, in the present model if another value is not specified). These boundary conditions require the surface density of tangential external forces equal zero. This means that the large-scale flow is controlled by internal processes inside the convection zone, not imposed externally. An equivalent formulation of the stress-free conditions as

$$\frac{\partial R_{r\vartheta}}{\partial\varphi} - \frac{\partial\left(\sin\vartheta R_{r\varphi}\right)}{\partial\vartheta} = 0, \qquad \frac{\partial R_{r\varphi}}{\partial\varphi} + \frac{\partial\left(\sin\vartheta R_{r\vartheta}\right)}{\partial\vartheta} = 0 \tag{20}$$

leads, in view of Equations (14), (17), and (18), to the conditions for the flow potentials:

$$\left(rU - 2W\right) + \Omega r^2 \times \times\left[\cos\vartheta\Lambda_0 + \left(\cos\vartheta/3 + 2\cos^3\vartheta/5\right)\Lambda_1\right] = 0, \qquad 2Q + rD = 0, \tag{21}$$

where U, Q, and D are the new dependent variables,

$$U=\frac{\partial W}{\partial r},\ Q=\frac{1}{\rho}\frac{\partial V}{\partial r},\ D=-\frac{\left(\hat{L}V\right)}{\rho r^2}-\frac{\partial Q}{\partial r}. \qquad (22)$$

The reason for introducing the new dependent variables is related to the numerical method of the model as explained below. The closed boundary condition, v_r=0, such that V=0, is also applied to both boundaries.

Spherically symmetric heat flux $F_r^{\rm conv}\left(r_1\right)=\delta F\left(r_1\right)$, enters the convection zone through the bottom boundary, where

$$F_r^{\rm conv}=-\rho T\chi_{\rm T}\left[\left(\phi\left(\Omega^*\right)+C_\chi\phi_\parallel\left(\Omega^*\right)\cos^2\vartheta\right)\frac{\partial S}{\partial r}-\right.$$
$$\left.-C_\chi\phi_\parallel\left(\Omega^*\right)\sin\vartheta\cos\vartheta\frac{1}{r}\frac{\partial S}{\partial\vartheta}\right]. \qquad (23)$$

The surface boundary radiates into surrounding space as a black body:

$$F_r^{\rm conv}\left(r_2\right)=\frac{L\left(r_2\right)}{4\pi r_2^2}\left(1+4\frac{S}{c_{\rm p}}\right). \qquad (24)$$

It is supposed in this equation that the thin layer between r_2 and the stellar surface is a perfect heat exchanger [Kitchatinov and Olemskoy, 2011].

1.4. Expansion in spherical functions and angular momentum conservation

Boundary conditions (20) ensure conservation of angular momentum

$$\mathbf{M}=\int_{r_1}^{r_2}\int_0^{\pi}\int_0^{2\pi}\rho r^2\sin\vartheta\left(\mathbf{r}\times\mathbf{v}\right)d\varphi d\vartheta dr. \qquad (25)$$

The formulation of this conservation law for the rotating reference frame has some specifics. Consider a rotating Cartesian reference frame with the rotation axis z and equatorial plane (x,y). Let the longitude φ in (25) be measured from the x-axis. Differentiate angular momentum (25) on time, substitute $\partial\mathbf{v}/\partial t$ from Equation (2), and integrate the resulting equation by parts. This gives

$$\dot{M}_z=0,\ \dot{M}_x=\Omega M_y,\ \dot{M}_y=-\Omega M_x. \qquad (26)$$

M_z and the absolute value $M_\perp=\sqrt{M_x^2+M_y^2}$ of the angular momentum normal to the rotation axis do not change with time. The conservation law can be used to control numerical solutions.

The angular momentum equations can be simplified by an expansion in spherical functions. Velocity expression (18) and the equations for the flow potentials (see Appendix) contain $\hat{L}$-operator (19) in multiple. It is therefore convenient to apply expansion in terms of the eigenfunctions $Y_{l,m}\left(\vartheta,\varphi\right)$ of this operator,

$$\overline{Y}_{l,m}\left(\vartheta,\varphi\right)=2\sin\left(m\varphi\right)\overline{P}_l^{|m|}\left(\cos\vartheta\right)\ \text{for}\ m<0,$$
$$\overline{Y}_{l,m}\left(\vartheta,\varphi\right)=\sqrt{2}\overline{P}_l^0\left(\cos\vartheta\right)\ \text{for}\ m=0, \qquad (27)$$
$$\overline{Y}_{l,m}\left(\vartheta,\varphi\right)=2\cos\left(m\varphi\right)\overline{P}_l^m\left(\cos\vartheta\right)\ \text{for}\ m>0,$$

where overlines mean the normalized functions. In particular, for the normalized adjoint Legendre polynomials $\overline{P}_l^{|m|}$, it means that $\int_0^{\pi}\left(\overline{P}_l^{|m|}\left(\cos\vartheta\right)\right)^2\sin\vartheta d\vartheta=1$.

The toroidal flow potential W is expanded as follows,

$$W\left(\mathbf{r},t\right)=\sum_{m=-M}^{M}\sum_{l=l_{\min}}^{l_{\max}}W_{l,m}\left(r,t\right)\overline{Y}_{l,m}\left(\vartheta,\varphi\right) \qquad (28)$$

and the same for other flow potentials and the entropy. In this equation, $l_{\min}=|m|$ for the entropy and $l_{\min}=\max\left(|m|,1\right)$ for the flow potentials, $l_{\max}=L+\max\left(|m|,1\right)-1$, M and L are the model parameters controlling the number of harmonics in decomposition (28). A peculiarity of Equation (28) is that the maximum azimuthal M and meridional L wave numbers are not mutually dependent and can assume arbitrary values. This imparts flexibility to the model that can be used not only for nonlinear 3D numerical experiments, but also for simulating the axisymmetric (M=0) flows and for analyzing the axisymmetric flow stability to disturbances with moderate m.

Substitution of (28) into (25) shows that only the modes with l=1 contribute to the angular momentum:

$$\left(M_x,M_y,M_z\right)=$$
$$=-\frac{8\pi}{\sqrt{3}}\int_{r_1}^{r_2}\rho r^2\left(W_{1,1}\left(r\right),-W_{1,-1}\left(r\right),W_{1,0}\left(r\right)\right)dr. \qquad (29)$$

Decomposition (28) also leads to a useful expression for the total kinetic energy $E_{\rm k}=\int\rho v^2d^3\mathbf{r}/2$,

$$E_{\mathbf{k}}=2\pi\sum_{l,m}l\left(l+1\right)\times$$
$$\times\int_{r_1}^{r_2}\left[\frac{l\left(l+1\right)}{\rho r^2}V_{l,m}^2\left(r\right)+\rho Q_{l,m}^2\left(r\right)+\rho W_{l,m}^2\left(r\right)\right]dr, \qquad (30)$$

which suggests that the kinetic energy is not only a superposition of independent contributions of the poloidal and toroidal parts of the flow but also splits into the contributions of individual harmonics from the flow expansion in spherical functions. It should be noted that this superposition holds globally for the total energy, but it is not valid for the local energy density.

Equations (29) and (30) can be applied to diagnostics of numerical computations.

2. NUMERICAL METHOD

Decomposition (28) in spherical functions leads to a system of partial differential equations in two independent variables, t and r. The equations are solved numerically by finite difference methods.

The problem at hand has thin (Ekman) boundary layers [Durney, 1989]. The finite-difference grid in radius should therefore be denser near the boundaries. The grid of N points includes the boundaries r_1, r_2 and intermediate grid points

$$r_j=\frac{1}{2}\left[r_2+r_1-\left(r_2-r_1\right)\cos\left(\pi\frac{j-3/2}{N-2}\right)\right], \qquad (31)$$
$$2\le j\le N-1.$$

The grid is a linear transform of zeros of Chebyshev polynomials in the range of [–1, 1] to [r_1, r_2]. This finite-difference grid worked well in former 2D models

[Kitchatinov, Olemskoy, 2011, 2012]. It also permits computation of integrals (29) and (30) with high precision by the method of the Gauss-Chebyshev quadrature [Press et al., 1992]. Coefficients of the model equations depend on the stellar structure parameters. The parameters are computed with the MESA model [Paxton et al., 2011]. The MESA results are transformed into grid (31) by cubic spline interpolation. New dependent variables U, Q, and D (22) are introduced in order to simplify the finite-difference derivations. With these variables, the model equations include the first-order spatial derivatives only, and formulation of the equations for the midpoints between neighbouring grid points ensures second-order precision in radius.

The model is second-order accurate in time also. All terms in the equations except for the diffusive ones (viscosity and thermal diffusion) were advanced in time with the second-order Runge-Kutta method. Diffusion is treated with the Crank-Nicholson method [Press et al., 1992]. More specifically, the explicit diffusion scheme is applied with a weight of (1–q) and the implicit one – with weight q, where q is the model parameter, $0.5 \le q \le 1$ (the low bound follows from the numerical stability condition). q=0.501 in the model computations if another value is not stated. This q-value ensures numerical stability but is close to q=0.5 of the second-order accurate Crank-Nicholson scheme.

The time-step equals one percent of the rotation period, $\Delta t = 0.01 P_{\rm rot}$. The number of radial grid points N=31 gave a sufficiently good accuracy for the Sun with a rotation period $P_{\rm rot}$=25.4 days; increasing N beyond this number did not change noticeably the results. The presence of Ekman boundary layers demands an increase in N in proportion to $P_{\rm rot}^{-1/2}$ for shorter rotation periods.

3. FIRST RESULTS

The MESA model for a star of one solar mass and metallicity Z=0.02 gives R_*=1.003$R_\odot$ and luminosity L_*=0.999$L_\odot$ for the age of 4.6 Gyrs. The structure of this star was used in computations for the Sun.

Figure 3 shows relative deviation ε (1) from adiabatic stratification within the convection zone. In accord with the anelastic approximation [Lantz, Fan, 1999], radial inhomogeneity of thermodynamic parameters in the entire convection zone except for a thin near-surface layer is close to an adiabatic profile.

3.1. Relaxation to an axisymmetric steady state

Consider first the computations for the initial condition of zero flow (**v**=0) and latitude-independent entropy distribution (12). The maximum wave numbers in expansions (25) were L=21 and M=5, i.e. the computations permit deviations from axial symmetry.

As initial angular momentum (25) in our rotating reference frame is zero, it should remain so according to conservation rules (26). However, our numerical method is not conservative in angular momentum. Equations (26)

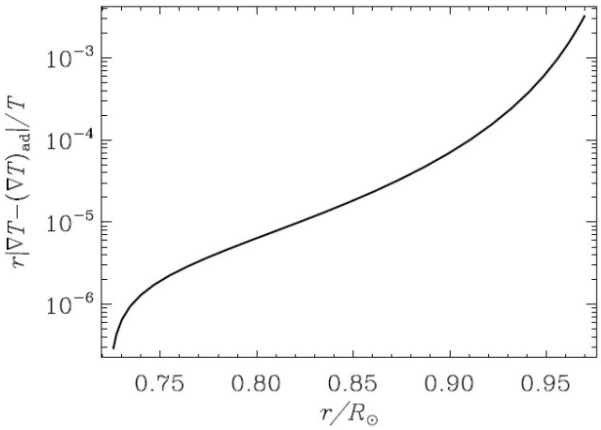

Figure 3. Normalized deviation from adiabatic stratification in the solar convection zone according to Equations (1) and (9)

were therefore violated in the course of the computations but the values of M_z и $M_\perp$ did not exceed 10^{-4} of the product M_0=$I\Omega$ of the convection zone momentum of inertia I with the angular velocity.

In the course of the runs, the large-scale flow emerges and then increases due to Λ-effect (14) and the baroclinic source of the poloidal flow (see Appendix). The heat transport anisotropy of Equation (11) induces the entropy dependence on latitude. Meanwhile, the flow and entropy conserve the axial symmetry of the initial state. This means that the "numerical noise" due to the finite precision of numerical computations does not produce non-axisymmetric disturbances in the proposed model.

An equatorially symmetric steady state is approached after the diffusive time R_*^2/ν (~10 years). The results are presented in Figures 4–6. The agreement with observations weakened somewhat compared to the axisymmetric steady model by Kitchatinov and Olemskoy [2011] but still remains rather close. Figure 4 shows the modelled differential rotation. For comparing with observations, the angular velocity Ω of the reference frame is added here to the computed rotation rate. The modelled surface rotation closely agrees with Doppler measurements by Snodgrass and Ulrich [1990]. The meridional flow of Figure 5 also agrees with seismological detections [Rajaguru, Antia, 2015; Gizon et al., 2020].

The temperature difference $\delta T = T\delta S / c_{\rm p}$ between the equator and poles is shown in Figure 6 as the function of radius r. The differential temperature is important for the thermo-rotational balance in the bulk of the convection zone and for meridional flow excitation near its boundaries [Hazra et al., 2023]. Note that the differential temperature $\delta T \simeq 1.4$ K on the upper boundary of the simulation domain does not equal to its value on the photosphere. If the layer from the upper boundary to the stellar surface is a perfect heat exchanger, as assumed in the model, then equal values have entropy disturbances $\delta S \propto \delta T / T$ at the upper boundary and the surface. The steep temperature decrease toward the surface then implies a "not measurable" surface differential temperature of order 0.01 Kelvin.

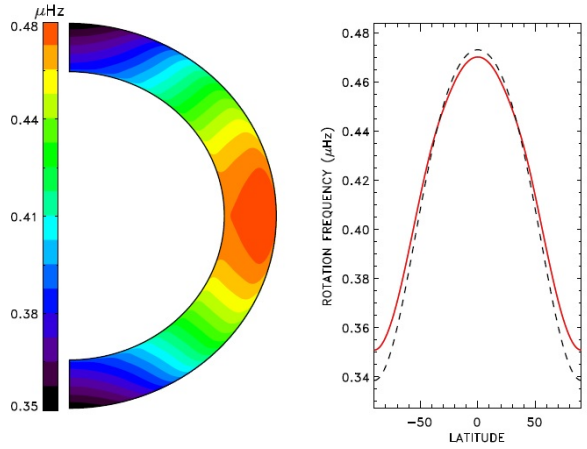

Figure 4. Differential rotation of the asymptotic axisymmetric state: angular velocity isolines (left) and the surface differential rotation (right). Full and dashed lines indicate the model results and Doppler measurements by Snodgrass and Ulrich [1990] respectively

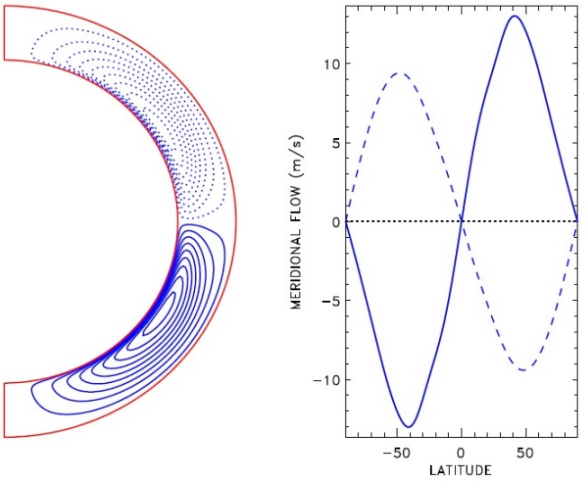

Figure 5. Left: Streamlines of the meridional flow after the model computation. Full and dotted lines show the clockwise and anticlockwise circulation respectively. Right: Meridional velocity on the surface (full line) and bottom (dashed) of the convection zone

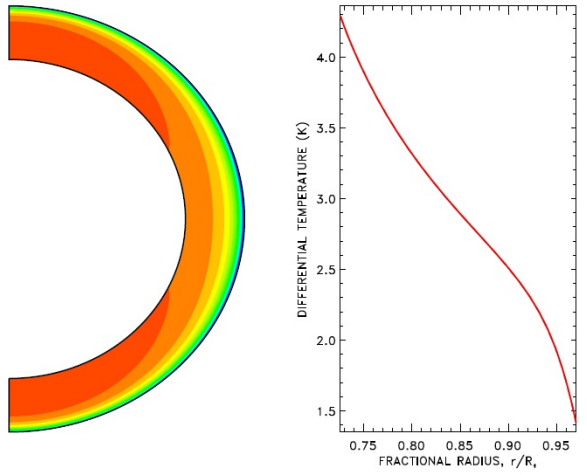

Figure 6. Entropy profile in the axisymmetric steady state. Left: Isentropic lines. Right: Differential temperature – temperature difference between poles and equator – as function of radius

3.2. Dynamics of non-axisymmetric disturbances

Other computations use a mixture of the steady axisymmetric solution (see Figures 4–6) with non-axisymmetric disturbances of the toroidal flow of $1 \le m \le 5$ and amplitude ~0.1 of its axially symmetric part as the initial condition. Nonlinear interactions cause the non-axisymmetric poloidal flow and entropy disturbances to emerge later on.

In the case of decaying deviations from axial symmetry, the computations would show eigenmodes of the model equations with finite m. However, the computations revealed a non-axisymmetric instability indicative of an internal contradiction in the mean-field hydrodynamics when applied to stellar convection zones. Non-axisymmetric disturbances initially grow with time. Then, the growth saturates at some amplitude of irregularly varying with time disturbances. The axisymmetric part of the solution also attains an irregularly varying part. This instability is not new [Rüdiger, Spahn, 1992; Tuominen et al., 1994]. By all probabilities, this instability is thermal convection. This is in particular indicated by the fact that the instability does not develop if radial velocity is put to zero, v_r=0, in the entropy equation. It is assumed in mean-field hydrodynamics that the role of turbulent convection is fully accounted for by introducing eddy transport coefficients. The presence of convective instability in the model evidences inconsistency of such an assumption: the eddy transport coefficients do not replace convection.

The present instability has been met in the axisymmetric model of the steady differential rotation [Kitchatinov, Olemskoy, 2011] as well. In the model, the instability was eliminated by applying a sufficiently large ratio $\alpha_{\rm MLT} = \ell / H_{\rm p}$ of the mixing length to the pressure scale height, and the closer was the upper boundary r_2 to the stellar surface, the larger $\alpha_{\rm MLT}$ value was required for stability. This means that instability is located near the surface, which has also been notified by Tuominen et al. [1994]. This can be explained by an increase in superadiabaticity toward the stellar surface (see Figure 3). An increase in the mixing length reduces entropy gradient (9) and increases diffusion (8). This is why an increase in $\alpha_{\rm MLT}$ suppresses the instability. It can be noted that reducing the mixing length near the base of the convection zone does not provoke the instability [Kitchatinov, Nepomnyashchikh, 2017]. In the axisymmetric models, $\alpha_{\rm MLT}$=2.2 ensures stability for $r_2 = 0.97 R_*$. This value of $\alpha_{\rm MLT}$ is also used in the present paper. The model is therefore stable with axial symmetry (see Figures 4–6). The dominant mode of rotating convection is, however, not axisymmetric (banana cells [Glatzmaier, Gilman, 1981]). Instability to non-axisymmetric disturbances therefore remains.

The mean-field hydrodynamics can probably be rectified from the discussed contradiction by allowance for the dependence of $\alpha_{\rm MLT}$ on radius following, e.g., from minimisation of total (kinetic plus thermal) energy of convection zone. Such a task should probably be a subject of a separate work. In this paper, the thermal con-

vection is excluded artificially by using a fixed steady entropy distribution obtained in the axisymmetric model (see Figure 6). Initial non-axisymmetric disturbances are then decaying with time.

The decay is clearly seen in Figure 7, where the kinetic energy of the disturbances of different m is shown in dependence on time, separately for toroidal and poloidal parts of the flow. As the non-axisymmetric disturbances decay, their nonlinear interactions weaken. The flow modes of different m then evolve independently because coefficients of the model equations do not depend on longitude. Eventually, the most slowly decaying eigenmode of the model equations survives for each m. The energy of an eigenmode depends on time as $\exp\left(-2t/\tau_m\right)$, where τ_m is the characteristic life-time of the eigenmode. These time dependences form strait lines in Figure 7. It takes a sufficiently long time for the longest living mode to emerge from the initial mixture of the eigenmodes. The eigenmodes' parameters are given in Table.

Recent observations [Löptien et al., 2018; Mandal et al., 2021; Mandal, Hanasoge, 2024] discovered *r*-modes [Saio, 1982] – horizontal vortices drifting in longitude – on the Sun. A distinctive feature of *r*-modes

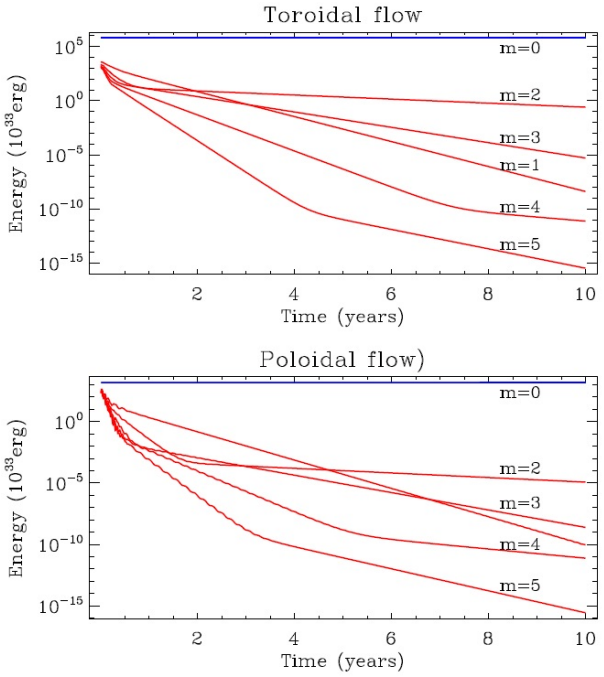

Figure 7. Kinetic energy (30) of the toroidal (top panel) and poloidal (bottom) parts of the flow for different azimuthal wave numbers m. Energy is given in units of 10^{33} erg

Parameters of non-axisymmetric eigenmodes of large-scale flow. Lifetime τ_m, toroidal-to-poloidal energy ratio $E_{\rm tor}/E_{\rm pol}$, and symmetry notations for the equator-symmetric (S) and antisymmetric (A) modes

m	τ_m, years	$E_{\rm tor}/E_{\rm pol}$	Symmetry
1	0.754	45.9	S
2	4.64	21200	A
3	1.22	2080	A
4	2.30	1.00	S
5	0.970	1.24	S

is a small value of radial displacements. It can be seen from Table that a relative small radial (poloidal) flow was found for m from 1 to 3. The flow patterns for eigenmodes with m=2 and 3 are demonstrated in Figures 8 and 9 respectively.

Toroidal vortex flows in these Figures are centered on the equator and have the so-called sectorial structure, i.e. they have no nodes of sign reversal in latitude. This is in qualitative agreement with observations made by Löptien et al. [2018]. But in view of the above contradiction, the results of this paper for non-axisymmetric flows are preliminary. We therefore refrain from more detailed comparison with observations.

CONCLUSION

This paper was aimed at extending the steady differential rotation models by allowing for variations with time and deviations from axial symmetry. The work suitability is justified by observations of large-scale vortices on the Sun and by a planned unification with dynamo models.

The new model for large-scale flows in convection zones of the Sun and stars has been developed in the framework of mean-field hydrodynamics and is realized as a numerical code for solving equations of hydrodynamics and heat transport. The numerical model combines

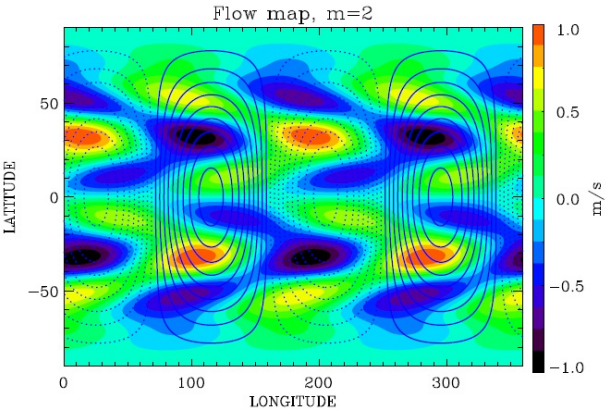

Figure 8. Flow pattern of the eigenmode with azimuthal wave number m=2 at radius $r = 0.9R_*$. Full (dotted) lines indicate streamlines of toroidal flow with clockwise (anticlockwise) circulation. Radial velocity is coded by color. Amplitude of the decaying flow is normalized to 1 m/s

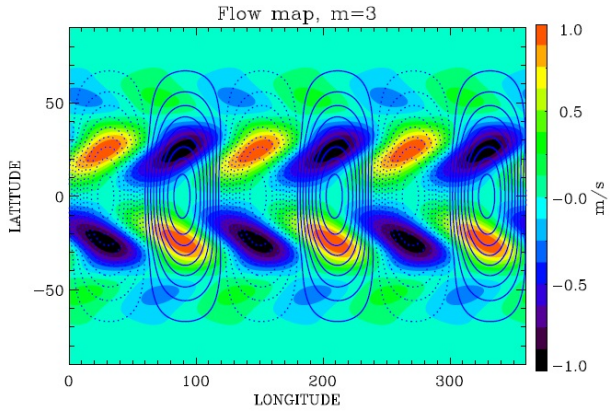

Figure 9. The same as in Figure 8 but for m=3

the spectral decomposition method in horizontal dimensions with second-order accurate finite difference methods in time and radius. This provides a reliable tool for further theoretical studies of the Sun and stars with external convection zones.

Our first computations have shown that the axially symmetric part of computed flow reproduces closely the differential rotation and meridional flow patterns detected by helioseismology. At the same time, computations of non-axisymmetric flows revealed an internal contradiction of mean-filed hydrodynamics in its applications to stellar convection zones, which calls for a revision of the mixing-length theory. The proposed model can and should be used in eliminating the contradiction. The first computations of non-axisymmetric flows have nevertheless demonstrated at least qualitative agreement with observations of large-scale Rossby waves on the Sun.

This work was financially supported by the Ministry of Science and High Education of the Russian Federation.

REFERENCES

Balona L.A., Abedigamba O.P. Differential rotation in K, G, F and A stars. *Monthly Notices of the Royal Astronomical Society*. 2016, vol. 461, iss. 1, pp. 497–506. DOI: 10.1093/mnras/stw1443.

Barnes J.R., Collier Cameron A., Donati J.-F., et al. The dependence of differential rotation on temperature and rotation. *Monthly Notices of the Royal Astronomical Society*. 2005, vol. 357, iss. 1, pp. L1–L5. DOI: 10.1111/j.1745-3933.2005.08587.x.

Brandenburg A., Elstner D., Masada Y., Pipin V. Turbulent processes and mean-field dynamo. *Space Sci. Rev*. 2023, vol. 219, iss. 7, id. 55. DOI: 10.1007/s11214-023-00999-3.

Chandrasekhar S. Hydrodynamic and hydromagnetic stability. Clarendon Press. Oxford. 1961.

Charbonneau P. Dynamo models of the solar cycle. *Living Reviews in Solar Physics*. 2020, vol. 17, iss. 1, id. 4. DOI: 10.1007/s41116-020-00025-6.

Charbonneau P., Sokoloff D. Evolution of solar and stellar dynamo theory. *Space Sci. Rev*. 2023, vol. 219, iss. 5, id. 35. DOI: 10.1007/s11214-023-00980-0.

Collier Cameron A., Donati J.-F. Doin' the twist: secular changes in the surface differential rotation on AB Doradus. *Monthly Notices of the Royal Astronomical S*ociety. 2002, vol. 329, iss. 1, pp. L23–L27. DOI: 10.1046/j.1365-8711.2002.05147.x.

Durney B.R. On the behavior of the angular velocity in the lower part of the solar convection zone. *Astrophys. J*. 1989, vol. 338, p. 509. DOI: 10.1086/167214.

Gizon L., Cameron R., Pourabdian M., et al. Meridional flow in the Sun's convection zone is a single cell in each hemisphere. *Science*. 2020, vol. 368, iss. 6498, p. 1469–1472. DOI: 10.1126/science.aaz7119.

Glatzmaier G.A., Gilman P.A. Compressible convection in a rotating spherical shell — Part two — a linear anelastic model. *Astrophys. J. Suppl*. 1981, vol. 45, pp. 351–380. DOI: 10.1086/190715.

Hazra G., Nandy D., Kitchatinov L., Choudhuri A.R. Mean field models of flux transport dynamo and meridional circulation in the Sun and stars. *Space Sci. Rev*. 2023, vol. 219, iss. 5, id. 39. DOI: 10.1007/s11214-023-00982-y.

Hotta H., Bekki Y., Gizon L., et al. Dynamics of large-scale solar flows. *Space Sci. Rev*. 2023, vol. 219, iss. 8, id. 77. DOI: 10.1007/s11214-023-01021-6.

Joyce M., Tayar J. A review of the mixing length theory of convection in 1D stellar modeling. *Galaxies*. 2023, vol. 11, iss. 3, id. 75. DOI: 10.3390/galaxies11030075.

Käpylä P.J., Browning M.K., Brun A.S., et al. Simulations of solar and stellar dynamos and their theoretical interpretation. *Space Sci. Rev*. 2023, vol. 219, iss. 7, id. 58. DOI: 10.1007/s11214-023-01005-6.

Karak B.B. Models for the long-term variations of solar activity. *Living Reviews in Solar Physics*. 2023, vol. 20, iss. 1, id.:3. DOI: 10.1007/s41116-023-00037-y.

Kichatinov L.L. Turbulent transport of angular momentum and differential rotation. *Geophysical and Astrophysical Fluid Dynamics*. 1986, vol. 35, iss. 1, pp. 93–110. DOI: 10.1080/03091928608245888.

Kichatinov L.L. A mechanism for differential rotation based on angular momentum transport by compressible convection. *Geophysical and Astrophysical Fluid Dynamics*. 1987, vol. 38, iss. 4, pp. 273–292. DOI: 10.1080/03091928708210111.

Kitchatinov L.L. The differential rotation of stars. *PhyU*. 2005, vol. 48, iss. 5, pp. 449–467. DOI: 10.1070/PU2005v048n05ABEH002099.

Kitchatinov L.L. The dependence of stellar activity cycles on effective temperature. *Res. Astron. Astrophys*. 2022, vol. 22, iss. 12, id. 125006. DOI: 10.1088/1674-4527/ac9780.

Kitchatinov L.L. Origin of the near-surface shear layer of solar rotation. *Astron Lett*. 2023, vol. 49, iss. 11, pp. 754–761. DOI: 10.1134/S106377372311004X.

Kitchatinov L.L., Nepomnyashchikh A.A. A joined model for solar dynamo and differential rotation. *Astron. Lett*. 2017, vol. 43, iss. 5, pp. 332–343. DOI: 10.1134/S106377371704003X.

Kitchatinov L.L., Olemskoy S.V. Differential rotation of main-sequence dwarfs and its dynamo efficiency. *Monthly Notices of the Royal Astronomical Society*. 2011, vol. 411, iss. 2, pp. 1059–1066. DOI: 10.1111/j.1365-2966.2010.17737.x.

Kitchatinov L.L., Olemskoy S.V. Differential rotation of main-sequence dwarfs: predicting the dependence on surface temperature and rotation rate. *Monthly Notices of the Royal Astronomical Society*. 2012, vol. 423, iss. 4, pp. 3344–3351. DOI: 10.1111/j.1365-2966.2012.21126.x.

Kitchatinov L.L., Rüdiger G. Differential rotation and meridional flow in the solar convection zone and beneath. *Astronomische Nachrichten*. 2005, vol. 326, iss. pp. 379–385. DOI: 10.1002/asna.200510368.

Kitchatinov L.L., Pipin V.V., Ruediger G. Turbulent viscosity, magnetic diffusivity, and heat conductivity under the influence of rotation and magnetic field. *Astronomische Nachrichten*. 1994, vol. 315, no. 2, pp. 157–170. DOI: 10.1002/asna.2103150205.

Kitiashvili I.N., Kosovichev A.G., Wray A.A., et al. Leptocline as a shallow substructure of near-surface shear layer in 3D radiative hydrodynamic simulation. *Monthly Notices of the Royal Astronomical Society*. 2023, vol. 518, iss. 1, pp. 504–512. DOI: 10.1093/mnras/stac2946.

Krause F., Rädler K.-H. Mean-field magnetohydrodynamics and dynamo theory. Akademie-Verlag, Berlin, 1980.

Lantz S.R., Fan Y. Anelastic magnetohydrodynamic equations for modeling solar and stellar convection zones. *Astrophys. J. Suppl*. 1999, vol. 121, iss. 1, pp. 247–264. DOI: 10.1086/31318.

Lebedinsky A.I. Rotation of the Sun. *SvA*. 1941, vol. 18. no. 1, pp. 10–25.

Löptien B., Gizon L., Birch A.C., et al. Global-scale equatorial Rossby waves as an essential component of solar internal dynamics. *Nature Astronomy*. 2018, vol. 2, pp. 568–573. DOI: 10.1038/s41550-018-0460-x.

Mandal K., Hanasoge S.M. Probing depth variations of solar inertial modes through normal mode coupling. *Astrophys. J*. 2024, vol. 967, iss. 1, id. 46. DOI: 10.3847/1538-4357/ad391b.

Mandal K., Hanasoge S.M., Gizon, L. Detection of Rossby modes with even azimuthal orders using helioseismic normal-mode coupling. *Astron. Astrophys.* 2021, vol. 652, id. A96. DOI: 10.1051/0004-6361/202141044.

Paxton B., Bildsten L., Dotter A., et al. Modules for experiments in stellar astrophysics (MESA). *Astrophys. J. Suppl.* 2011, vol. 192, iss. 1, id. 3. DOI: 10.1088/0067-0049/192/1/3.

Pipin V.V., Kosovichev A.G. On the origin of solar torsional oscillations and extended solar cycle. *Astrophys. J.* 2019, vol. 887, iss. 2, id. 215. DOI: 10.3847/1538-4357/ab5952.

Pipin V.V., Kosovichev A.G. Torsional oscillations in dynamo models with fluctuations and potential for helioseismic predictions of the solar cycles. *Astrophys. J.* 2020, vol. 900, iss. 1, id. 26. DOI: 10.3847/1538-4357/aba4ad.

Press W.H., Teukolsky S.A., Vetterling W.T., Flannery B.P. Numerical recipes. Cambridge University Press. 1992.

Rajaguru S.P., Antia H.M. Meridional circulation in the solar convection zone: time-distance helioseismic inferences from four years of HMI/SDO observations. *Astrophys. J.* 2015, vol. 813, iss. 2, id. 114. DOI: 10.1088/0004-637X/813/2/114.

Rüdiger G. Differential rotation and stellar convection. *Sun and Solar-Type Stars.* Akademie-Verlag, Berlin, 1989. 328 p.

Rüdiger G., Spahn F. On the stability of mean-field models of the solar convection zone. *Solar. Phys*. 1992, vol. 138, iss. 1, pp. 1–9. DOI: 10.1007/BF0014619.

Rüdiger G., Egorov P., Kitchatinov L.L., Küker M. The eddy heat-flux in rotating turbulent convection. *Astron. Astrophys.* 2005, vol. 431, pp. 345–352. DOI: 10.1051/0004-6361:20041670.

Saio H. R-mode oscillations in uniformly rotating stars. *Astrophys. J.* 1982, vol. 256, pp. 717–735. DOI: 10.1086/159945.

Schou J., Antia H.M., Basu S., et al. Helioseismic studies of differential rotation in the solar envelope by the solar oscillations investigation using the Michelson Doppler Imager. *Astrophys. J.* 1998, vol. 505, iss. 1, pp. 390–417. DOI: 10.1086/306146.

Snodgrass H.B., Ulrich R.K. Rotation of Doppler features in the solar photosphere. *Astrophys. J.* 1990, vol. 351, pp. 309–316. DOI: 10.1086/168467.

Thompson M.J., Toomre J., Anderson E.R., et al. Differential rotation and dynamics of the solar interior. *Science*. 1996, vol. 272, iss. 5266, pp. 1300–1305. DOI: 10.1126/science.272.5266.1300.

Tuominen I., Brandenburg A., Moss D., Rieutord M. Does solar differential rotation ARISE from a large scale instability? *Astron. Astrophys*. 1994, vol. 284, pp. 259–264.

Original Russian version: Kitchatinov L.L., published in Solnechno-zemnaya fizika. 2025, vol. 11, no. 4, pp. 5–16. DOI: 10.12737/szf-114202501.

How to cite this article

Kitchatinov L.L. Large-scale flow model for solar and stellar convection zones. *Sol.-Terr. Phys*. 2025, vol. 11, iss. 4, pp. 3–13. DOI: 10.12737/stp-114202501.

APPENDIX

EQUATIONS FOR THE TOROIDAL AND POLOIDAL FLOW PARTS

The equation for the toroidal part of the flow can be symbolically written as $r\mathbf{r}\cdot(\nabla\times$Equation (**2**)). In terms of scalar flow potentials (18) and new dependent variables (22), it reads

$$\frac{\partial\left(\hat{L}W\right)}{\partial t}=\frac{1}{\rho r^2}\frac{\partial}{\partial r}\left[\nu\rho r\hat{L}\left(rU-2W\right)\right]+\frac{\nu}{r^2}\left(\hat{L}+2\right)\left(\hat{L}W\right)+$$

$$+\Omega\hat{L}\left\{\frac{\cos^3\vartheta}{3\rho r^2}\frac{\partial}{\partial r}\left(\rho r^3\Lambda_1\right)-\frac{\cos\vartheta}{\rho r^2}\frac{\partial}{\partial r}\left(\rho r^3\Lambda_0\right)+\cos\vartheta\left(1-5\cos^2\vartheta/3\right)\Lambda_1\right\}-$$

$$-2\Omega\left\{\frac{\partial W}{\partial\varphi}+\sin\vartheta\frac{\partial}{\partial\vartheta}\left(Q+\frac{\hat{L}V}{r\rho}\right)-\cos\vartheta\left(\hat{L}Q-2\frac{\hat{L}V}{r\rho}\right)\right\}+$$

$$+\frac{1}{r^2\rho}\left\{\left(\hat{L}W\right)\frac{\partial\left(\hat{L}V\right)}{\partial r}-\left(\hat{L}V\right)\frac{\partial\left(\hat{L}W\right)}{\partial r}+\frac{\partial\left(\hat{L}W\right)}{\partial\vartheta}\frac{\partial^2V}{\partial\vartheta\partial r}-\frac{\partial\left(\hat{L}V\right)}{\partial\vartheta}\frac{\partial^2W}{\partial\vartheta\partial r}\right\}+$$

$$+\frac{1}{r^2\sin\vartheta}\left\{\frac{\partial W}{\partial\varphi}\frac{\partial\left(\hat{L}W\right)}{\partial\vartheta}-\frac{\partial W}{\partial\vartheta}\frac{\partial\left(\hat{L}W\right)}{\partial\varphi}+\frac{1}{\rho}\frac{\partial\left(\hat{L}V\right)}{\partial\varphi}\frac{\partial D}{\partial\vartheta}-\frac{1}{\rho}\frac{\partial\left(\hat{L}V\right)}{\partial\vartheta}\frac{\partial D}{\partial\varphi}\right\}+$$

$$+\frac{1}{r^2\rho\sin^2\vartheta}\left\{\frac{\partial\left(\hat{L}W\right)}{\partial\varphi}\frac{\partial^2V}{\partial\varphi\partial r}-\frac{\partial\left(\hat{L}V\right)}{\partial\varphi}\frac{\partial^2W}{\partial\varphi\partial r}\right\}.$$

The two first terms on the right side of the equation are the contributions of turbulent viscosity. The next term in the curly brackets account for the Λ-effect, the next curly brackets stand for the Coriolis force, and all further terms represent the nonlinearities. Note that with using new dependent variables (22), the equation contains only first-order derivatives in radius. This is what the new variables were introduced for.

The symbolic form of the equation for the poloidal flow, $r\mathbf{r}\cdot[\nabla\times(\nabla\times\text{Equation }(\mathbf{2})]$, is more complicated compared with the toroidal one. Accordingly, the equation in terms of the flow potentials is more bulky:

$$\frac{\partial\left(\hat{L}D\right)}{\partial t}=\hat{L}^2\left\{\frac{\nu}{r^2}D+\frac{2\nu+\mu}{\rho^3 r^2}\left(\frac{d\rho}{dr}\right)^2 V-\frac{2}{\rho^2}\frac{d\left(\rho\nu\right)}{dr}\frac{\partial}{\partial r}\left(\frac{V}{r^2}\right)\right\}+\hat{L}\frac{\partial F}{\partial r}-\frac{g}{c_p}\hat{L}S-$$

$$-2\Omega\left\{\frac{\partial D}{\partial\varphi}-\frac{1}{\rho r^2}\frac{d\rho}{dr}\frac{\partial\left(\hat{L}V\right)}{\partial\varphi}-\cos\vartheta\hat{L}U+\sin\vartheta\frac{\partial U}{\partial\vartheta}+\frac{1}{r}\hat{L}\left(\sin\vartheta\frac{\partial W}{\partial\vartheta}\right)\right\}+$$

$$+\frac{1}{r^2}\hat{L}\left\{\frac{\partial Q}{\partial\vartheta}\frac{\partial D}{\partial\vartheta}-\frac{\partial W}{\partial\vartheta}\frac{\partial U}{\partial\vartheta}+\frac{1}{\sin^2\vartheta}\frac{\partial Q}{\partial\varphi}\frac{\partial D}{\partial\varphi}-\frac{1}{\sin^2\vartheta}\frac{\partial W}{\partial\varphi}\frac{\partial U}{\partial\varphi}\right\}+$$

$$+\frac{1}{r^2}\hat{L}\left\{\frac{1}{\sin\vartheta}\left(\frac{\partial Q}{\partial\varphi}\frac{\partial U}{\partial\vartheta}-\frac{\partial U}{\partial\varphi}\frac{\partial Q}{\partial\vartheta}+\frac{\partial W}{\partial\varphi}\frac{\partial D}{\partial\vartheta}-\frac{\partial D}{\partial\varphi}\frac{\partial W}{\partial\vartheta}\right)\right\}+$$

$$+\frac{\partial}{\partial r}\frac{1}{r^2}\left\{\left(\hat{L}W\right)^2-\frac{1}{\rho}\left(\hat{L}D\right)\left(\hat{L}V\right)+\frac{\partial W}{\partial\vartheta}\frac{\partial\left(\hat{L}W\right)}{\partial\vartheta}-\frac{\partial D}{\partial\vartheta}\frac{\partial\left(\hat{L}V\right)}{\partial\vartheta}\right\}+$$

$$+\frac{\partial}{\partial r}\frac{1}{r^2\sin\vartheta}\left\{\frac{\partial\left(\hat{L}W\right)}{\partial\varphi}\frac{\partial Q}{\partial\vartheta}-\frac{\partial\left(\hat{L}W\right)}{\partial\vartheta}\frac{\partial Q}{\partial\varphi}+\frac{1}{\rho}\frac{\partial U}{\partial\varphi}\frac{\partial\left(\hat{L}V\right)}{\partial\vartheta}-\frac{1}{\rho}\frac{\partial U}{\partial\vartheta}\frac{\partial\left(\hat{L}V\right)}{\partial\varphi}\right\}+$$

$$+\frac{\partial}{\partial r}\frac{1}{r^2\sin^2\vartheta}\left\{\frac{\partial W}{\partial\varphi}\frac{\partial\left(\hat{L}W\right)}{\partial\varphi}-\frac{1}{\rho}\frac{\partial D}{\partial\varphi}\frac{\partial\left(\hat{L}V\right)}{\partial\varphi}\right\}.$$

In this equation, $F=\frac{1}{\rho}\frac{\partial\left(\rho\nu D\right)}{\partial r}+\frac{2}{\rho r}\frac{d\left(\rho\nu\right)}{dr}\left(Q+\frac{\hat{L}V}{\rho r}\right)$ is one more dependent variable in addition to (22). The term including the entropy is the baroclinic source of the poloidal flow.